GRAPHENE BIOINTERFACE FOR CARDIAC ARRHYTHMIA DIAGNOSIS AND TREATMENT

Zexu Lin[1]*, Dmitry Kireev[2,3]*, Ning Liu[2]*, Shubham Gupta[1], Jessica LaPaino[4], Sofian N. Obaid[1], Zhiyuan Chen[1], Deji Akinwande[2,3], Igor R. Efimov[1,5,6]

[1] Department of Biomedical Engineering, The George Washington University, Washington, DC, 20052, USA
[2] Department of Electrical and Computer Engineering, The University of Texas at Austin, Austin, TX, USA
[3] Microelectronics Research Center, The University of Texas at Austin, Texas, 78758 USA
[4] MedStar Georgetown University Hospital, Washington, DC, 20007, USA
[5] Department of Biomedical Engineering, Northwestern University, Evanston, IL 60208
[6] Department of Medicine (Cardiology), Northwestern University, Chicago, IL 60611

* These authors contributed equally

Corresponding authors: igor.efimov@northwestern.edu and d.kireev@utexas.edu

ABSTRACT

The human heart is an efficient electromechanical pump which provides oxygen and nutrients to all human organs. Each heartbeat is ignited and synchronized by an electrical action potential initiating and rapidly propagating through the heart's electrical system. Cardiovascular diseases, a leading cause of death in humans, disrupt this synchronous excitation. Heart rhythm disorders, known as arrhythmias, are particularly deadly. Cardiac arrhythmias are primarily treated by implantable pacemakers and defibrillators because pharmacological treatments are mostly ineffective. In this work, we report on graphene-only cardiac pacemakers as advanced cardiac biointerfaces. Leveraging sub-micrometer thick tissue-conformable graphene arrays, we are able to sense from and stimulate the heart, altering its functions, suggesting that the devices can be used for high-density functional interfacing with the heart. The arrays show effective electrochemical properties, namely interface impedance down to 40 Ohm×cm^2, charge storage capacity up to 63.7 mC/cm^2, and charge injection capacity up to 704 μC/cm^2. Transparency of the structures allows for simultaneous optical mapping of cardiac action potentials and calcium transients while performing electrical measurements. Upon validating the graphene-based cardiac pacing in *ex vivo* mouse hearts, we performed *in vivo* cardiac pacing in a rat model with clinically induced arrhythmia. The condition was successfully diagnosed and treated using graphene biointerfaces.

Introduction

The heart is the first organ to function after conception, and it pumps blood carrying oxygen and nutrients to all organs without interruption until death. Normal cardiac function is orchestrated by a periodic electrical wave of excitation propagating from the natural cardiac pacemaker, the sinoatrial node, through every myocyte electrically coupled to their neighbors. This electrical propagation is commonly documented by an electrocardiogram (ECG). Various cardiovascular, autonomic, and metabolic diseases lead to disruption of normal heart rhythm known as cardiac arrhythmia, which could be deadly unless treated by electrical stimulation applied to the heart muscle within 10 minutes. Current automated antiarrhythmic therapies, implantable pacemakers, and defibrillators, are effective. However, they are still based on stiff and rigid materials that do not conform well to the soft and dynamically contracting cardiac tissue, resulting in deteriorating performance, limited lifetime, and repeated surgical procedures. Leads of implanted cardiac pacemakers and defibrillators may fail, cause tissue inflammation and endocardial fibrosis[1,2] which can result in pacemakers malfunctioning and even cause lethal events[3–5]. Conventional, widely used metal-based devices for cardiac electrophysiology (EP) studies have shortcomings manifested in mechanical, chemical, and electrical tissue-material mismatch[3,6–8].

The most advanced approaches to emerging cardiac implants are based on soft organ-conformal bioelectronics[9–15]. The soft bioelectronics tools specifically made for cardiovascular applications have enabled more profound understanding of cardiac physiology and play an important role in clinical diagnosis and treatment of diseases such as metabolic dysfunction, heart failure, and arrhythmia[11,16–19]. Several considerable achievements have been reported, such as optogenetic cardiac pacing *via* a fully implantable battery-free pacemaker[16], cardiac ablation *via* a catheter-integrated multi-functional soft electronic array[17], and bioresorbable transient pacemaker controlled by a wearable device network[18,20,21].

Different soft electronics approaches have been reported integrating components based on meshes of metal nanowires and nanoribbons[19,22], three-dimensional graphene[23], iridium oxide[24], platinum[25], and PEDOT:PSS[26]. These are just some of the most commonly used elements of nanobioelectronics that have been explored to realize functional electrodes and transistors for electrical recording and stimulation of the heart tissue. However, despite the remarkable progress,

current fabrication methods still have some limitations, such as complex procedures, limited fabrication materials, and high labor and time costs.

As a remarkable two-dimensional (2D) material with sub-nanometer thickness[27], graphene possesses outstanding bioelectronics-relevant properties such as optical transparency (~97% for visible light)[28], strength (130 GPa)[29], stretchability (~15%)[30], and biocompatibility[31,32]. Therefore, graphene is a promising building block for soft bioelectronics[33] and has been reported to fabricate cardiopatches[34], flexible microelectrodes[35,36] and microprobes[37–39] for electrical activities monitoring and stimulation in cardiac and neural cellular research. Recently, a cost- and time-effective fabrication protocol using off-the-shelf methods to create skin graphene electronic tattoos (GETs) of various shapes has also been reported[40]. A combination of these approaches could potentially help develop graphene-based biointerfaces for the intact heart, including clinical applications in implantable and interventional cardiac therapies.

In this work, we approach the problem by leveraging atomically thin electronic graphene tattoos as soft, tissue imperceptible, and transparent bi-directional bioelectronic interfaces. *Ex vivo* tests in a mouse model demonstrate the capability of cardiac electrogram recording and rhythm capturing and pacing by GET-electrodes. Compatibility of the transparent GET-electrodes with cardiac optical mapping technique allows accurate measurement of electrophysiology restitution properties of the heart that is critical to cardiac function. *In vivo* tests in a rat model using an array of GETs indicate the potential of high-density electrical mapping from multiple locations on a beating heart. The successful ventricular rhythm restoration during the atrioventricular block (AV block), a common arrhythmia, indicates the clinical potential of treating arrhythmias using GET-electrodes that can withstand the dynamic motion of the *in vivo* beating heart. These results support the use of transparent and flexible GET-electrodes fabricated by a simple and cost-effective method for applications in cardiac transvenous EP studies and ablation arrhythmia therapy, and different implantable anti-arrhythmia devices.

Results & Discussion

Graphene cardiac tattoos

The graphene biointerface technology reported in this work is derived from the previously introduced GETs[40–42], additionally supported with two layers of ultrathin elastomer. The top layer of the elastomer features an electrode opening (see Fig. 1) with a diameter varying between 1 and 3 mm. An ultrathin (10 μm) adhesive, elastic, and conductive gold tape was leveraged as the hybrid interconnect: soft enough for contacting graphene yet hard and robust enough for external connection with measuring and stimulating electronics. Furthermore, to ensure that graphene does not affect biological processes *in vivo* or *ex vivo*, the GETs were modified with micrometer-sized holes, allowing for efficient water transport[43]. Besides, the holey GETs feature a unique tendency toward forming an electrically robust interface with the conductive material on both sides/planes of the GET (graphene plane and holey PMMA plane), which has given us the freedom to create the hybrid cardiac tattoo samples. In this work, we used 3-layer-GETs as they provide the most reproducible qualities, including lowest sheet resistance and lower interface impedance.

A simple, easy-to-replicate method (Fig. 1a) was developed to produce GET-electrodes (Fig. 1b) for a direct electrical interface with the heart (Fig. 1c) that only requires two steps. First – spin coating of poly(vinyl alcohol) (PVA) and silicone acted as the temporary supporting layer and flexible encapsulating layer, respectively. Second – defining different electrode window patterns with biopsy punches of various sizes (diameter 1-3mm). A GET-electrode consists of three primary layers with different functional purposes (Fig. 1a-b) involving (i) transparent and flexible encapsulating films, (ii) GETs that could come with various shapes based on anatomical and device requirements, and (iii) a flexible and ultrathin conductive gold tape that acted as the interconnect between GET-electrodes and data acquisition and stimulation hardware. The lightweight and soft GET-electrode could easily conform to the curvature of small anatomical structures of a mouse heart (Fig. 1c).

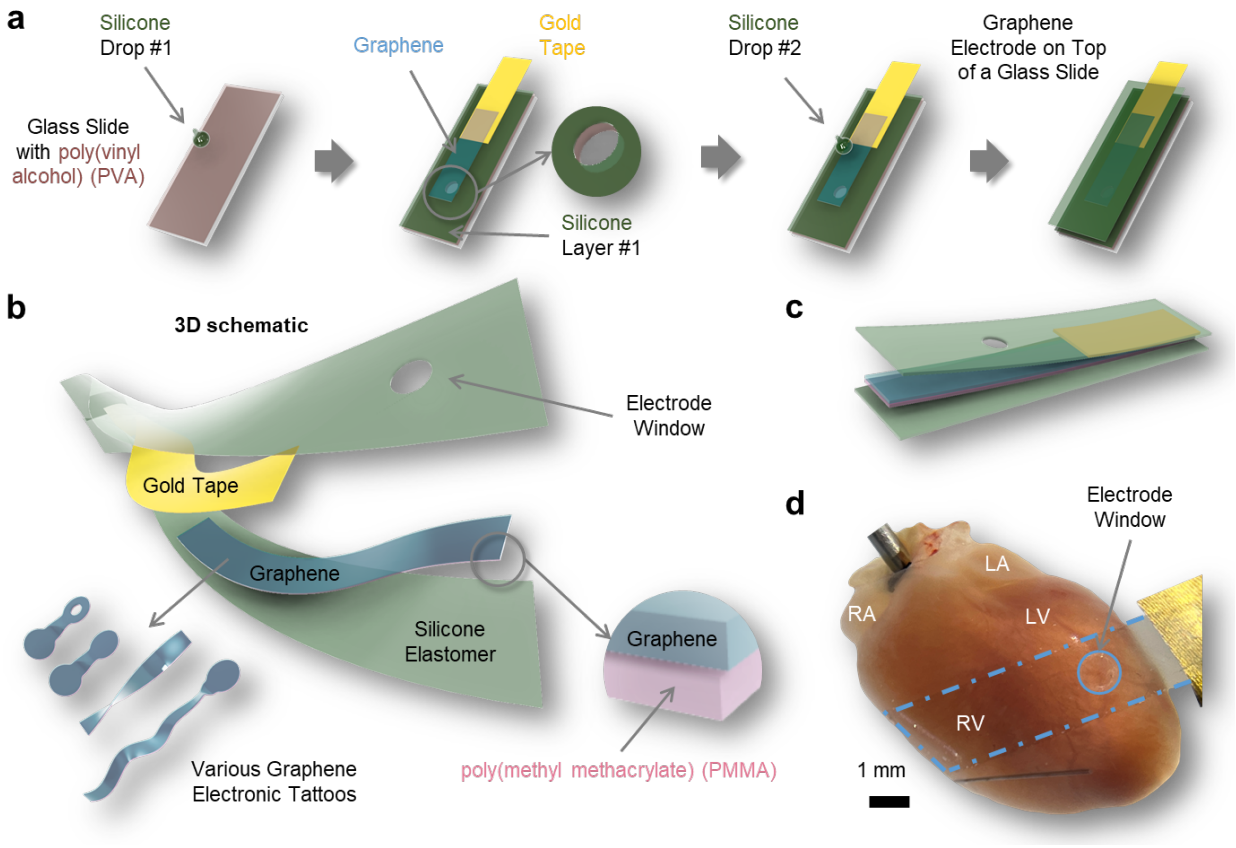

Figure 1 Device fabrication process. ***a***, *Step-by-step schematic of the fabrication method for GET-electrodes.* ***b***, *3D schematic of the Cardiac Graphene Tattoo featuring atomically thin and transparent graphene (blue), supported by 200nm thick PMMA (pink) and silicone elastomer (light green), and gold tape (yellow) is used to connect to graphene. Diameter of the electrode window (i.e., the exposure area for graphene contact with tissue) can be configured by using biopsy punches of various sizes (1-3mm). The morphology of graphene can be adjusted based on performance requirements. The conductive gold tape is the inter-connector between graphene electrodes and data acquisition hardware. The silicone elastomer acts as the protecting and insulating layers for graphene.* ***c***, *Schematic of the side view of a typical graphene electrode.* ***d***, *Photograph of a graphene electrode (1 mm unipolar electrode window) on a mouse heart. The edges of graphene and the electrode opening window are highlighted with blue dashed lines since graphene is almost fully transparent. RA, right atrium; LA, left atrium; RV, right ventricle; LV, left ventricle.*

Electrical and electrochemical characterization of graphene electrodes

To ensure reliability *ex vivo* and *in vivo*, the GET cardiac patches were first tested for their electrochemical performance. Large surface area GETs have been made for initial tests, typically 15 to 18 mm^2. The large GETs were made in three configurations: monolayer graphene (1L),

bilayer graphene (2L), and trilayer graphene (3L, see Methods for fabrication details). As one can see from Fig. 2a, there is a clear trend in decreasing of the electrochemical impedance of the devices with a larger number of graphene layers in the stack. On average, the 3L-GETs have an interface impedance of 2.5±0.7 kOhm at 1kHz (see Fig. S1) or area-normalized impedance of 345±151 Ohm×cm^2 (see Fig. 2b). Interestingly, the small devices with electrode openings of 1mm, 1.5mm, 2mm, and 3mm in diameter show a downwards trend of reducing normalized impedance with smaller electrode openings, suggesting that smaller electrodes are more efficient (see Fig. 2b and Table S2). This efficiency is likely to come from the larger edge/area ratio of the smaller electrode, and potentially the charge transfer is more efficient through the edges rather than that middle part of the electrodes.

The average value of area-normalized impedance at 1 kHz for 1mm opening 3L GETs is 40±13 Ohm×cm^2, which is on par and even exceeds that value of highly conducting $PtTe_2$ and gold e-tattoos[44]. The GETs exhibited outstanding stability and no degradation of the properties over a few days and a week of measurements (see Fig. S2). To move forward with the electrochemical characterization of the cardiac graphene tattoos, we characterized their electrochemical stability and determined their so-called water window. As well-known from the previous works, graphene has a very wide water window, which we corroborated in this work. We have been able to safely perform cyclic voltammetry (CV, see Fig. S3) measurements in the range of applied potential between -0.9V and +1.2V, which defines the graphene water window[37,45]. Furthermore, we have found no significant dependency of the water window per electrode opening area or per number of graphene layers (see Figure S3). The CV measurements, performed at 5 mV/sec rate, have been used to estimate another essential figure-of-merit of microelectrodes, their charge storage capacity (CSC). Similar to the case of interface impedance, the CSC follows a similar trend (see Fig. 2c), where area-normalized values are much larger for the smaller electrodes. For large devices, the average CSC is estimated in the range of 2-5 mC/cm^2. At the same time, the value is almost an order of magnitude higher, 63.7±14.6 mC/cm^2, for smaller electrodes, with ~1mm diameter opening (see Table S3 for details). Finally, the essential value for effective stimulation of electrogenic tissue is the charge injection capacity (CIC) of the electrodes. For this purpose, the charge-balanced measurements with constant-current pulses were applied to the electrodes. The resulting voltage transient for various pulse amplitudes and pulse widths are shown in Fig. 2d.

Extracting the CIC capacity is giving us a somewhat similar performance for 1L, 2L, and 3L large GETs, in the range of 60-90 μC/cm^2, with the values drastically increasing for smaller devices (see Fig. 3e), reaching up to 704±144 μC/cm^2 for electrodes with ~1mm diameter opening (see Table S4 for details). One can note a slight upwards trend with increasing the number of layers, suggesting that multilayer graphene helps in out-of-plane charge injection. The recorded properties for large devices are in good accordance with other works[46], while the superior performance measured for small GET-arrays is unprecedented. When put in perspective (see Table S1), the graphene electrodes are the thinnest made biointerfaces with the lowest (for graphene) interface impedance. Only a handful of works, mainly utilizing PEDOT and porous metals, can compete with the GETs. The same trend can be found for CSC and CIC, with the exception of composite multi-coated electrodes (*e.g.,* CNTs+porous Pt).

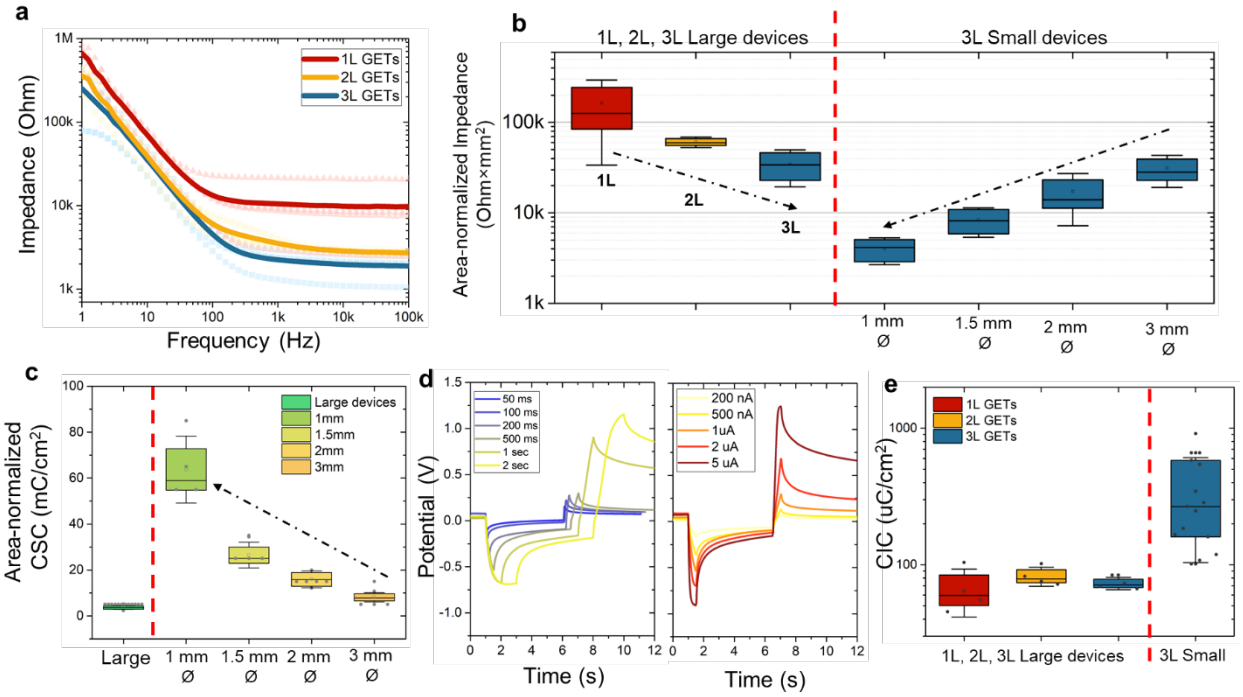

Figure 2 Electrochemical Performance of the GET arrays. ***a***, *Bode plot of the electrochemical impedance of the large graphene tattoos, made of 1L (red), 2L (yellow), and 3L (blue) graphene. Shaded symbols represent individual devices, and solid lines represent their average.* ***b***, *Area-normalized impedance of large GETs with 1L, 2L, and 3L configurations, and small GETs with 1mm, 1.5mm, 2mm, and 3mm electrode diameters.* ***c***, *Area-normalized charge storage capacity of the large and small GETs of different electrode opening dimensions.* ***d***, *The voltage transients for a variety of current widths (blue-to-yellow) with fixed amplitude and a set of different transients for various amplitudes (yellow to red)*

with fixed width. ***e****, The area-normalized charge injection capacity for GETs of different dimensions and number of layers. The box represents 25% and 75% with a mean, and the outliers are ±SD.*

Ex vivo cardiac electrophysiology sensing and actuating characterization

Upon completion of electrochemical characterization of the GET-electrodes, they were applied for monitoring cardiac electrical activity in an *ex vivo* Langendorff-perfused mouse heart model where the electrogram recorded by graphene (gEG) was compared with the traditional far-field ECG simultaneously recorded in the perfusion bath (Fig. 3a). The ECG was recorded from three sensing electrodes in the ECG lead II position. The gEG was recorded from a 2-sensing electrodes setup. The GET-electrodes came with both unipolar (1-, 1.5-, and 2 mm electrode windows) and bipolar (1 mm electrode window, window pitch distance 2 mm) setups. In the unipolar sensing and actuating mode, the same GET-electrode was used as the positive (+) electrode paired with another negative (-) electrode. In the bipolar mode, the two graphene electrodes were used as (+) and (-) electrodes, respectively. The simultaneously recorded ECG and gEG (Fig. 3b-c) showed a good temporal correlation between R waves and elapsed time between two successive R waves (RR interval, inversely related to heart rate) (Fig. 3d). Because the GET-electrode recorded local electrogram, the P waves were absent from gEG signals (Fig. 3c), present in ECG, which characterizes whole heart electrophysiology. The signal-to-noise ratio (SNR) was compared (Fig. 3e) for gEG recorded from unipolar GET-electrodes with various window sizes. We found that 1 mm samples show comparable performance to the control Pt electrodes. At the same time, there was a statistically significant decrease in the SNR of gEG recordings between the 1 mm and 2 mm group. Only in the 2 mm group, the gEG SNR was significantly lower than the control ECG SNR. This experimental data correlates with the data shown in Fig. 2b-c, where smaller diameter electrode arrays have featured superior interface impedance, charge storage, and charge injection capacities. Cardiac actuating was also achieved by connecting the GET-electrode to the cardiac stimulator (PowerLab 26T, ADInstruments). Cardiac pacing resulted in a faster heart rate, and pacing artifacts were followed by a wide QRS complex with increased amplitude, as commonly observed in patients with an implantable pacemaker (Fig. 3f). The *ex vivo* pacing strength-duration curve was characterized for various GET-electrodes along with a custom bipolar platinum electrode that served as the reference since it is always the electrode our lab uses for optical mapping studies (Fig. 3g, and Table S5 for details). The choices of stimulating pulses duration

included both animal research related value (*e.g.,* 2 ms for optical mapping studies) and clinically relevant pacing duration (*i.e.,* from 0.1 to 0.5 ms)[47–49].

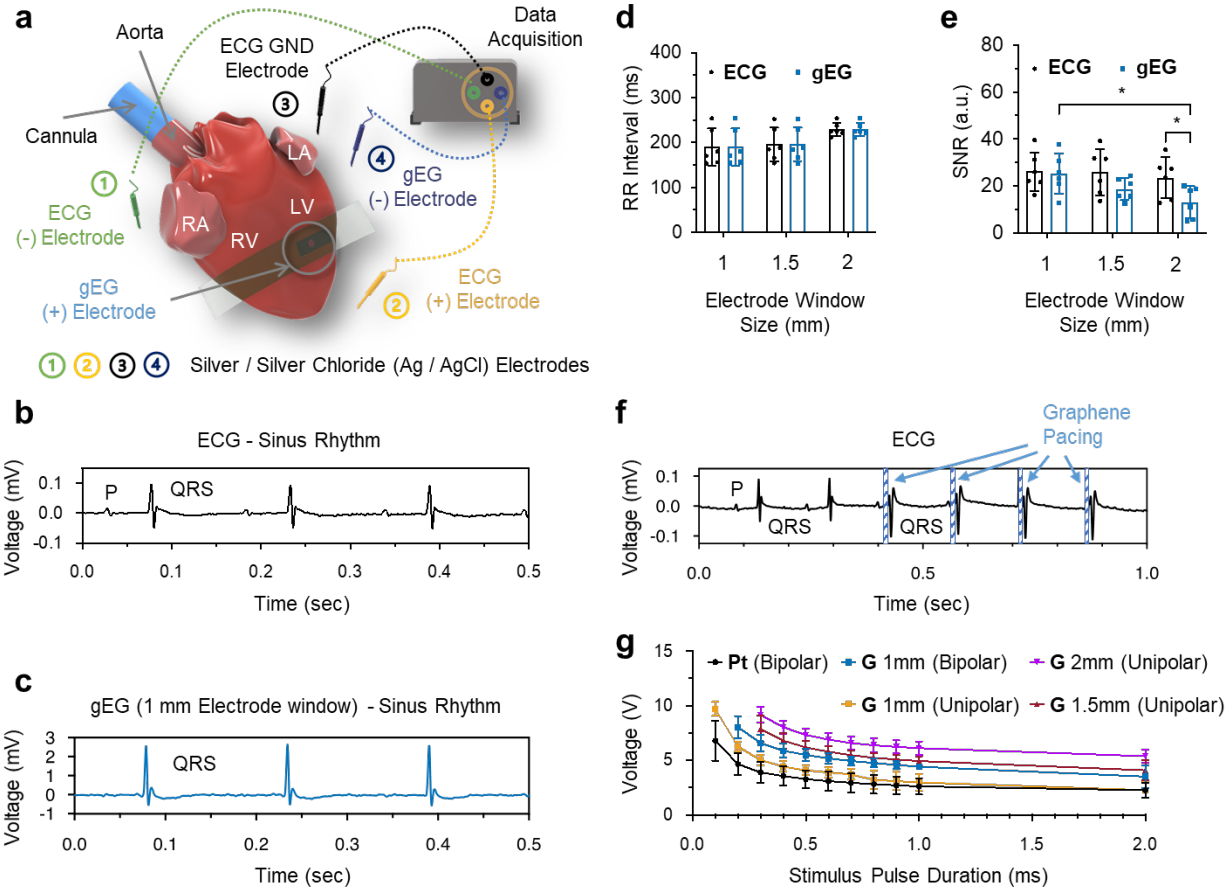

Figure 3 Ex vivo cardiac electrophysiology sensing and pacing with GETs. a, *Schematic of the ex vivo study setup. The GET-electrode was placed on a Langendorff-perfused mouse heart at the anterior side of the left ventricular surface. Far-field pseudo-ECG (ECG) was recorded using a 3-sensing electrodes setup. Graphene electrogram (gEG, blue) was recorded using a 2-sensing electrodes setup.* ***b-c,*** *Simultaneously recorded ECG* ***(b****, black****)*** *and gEG* ***(c****, blue****)*** *at natural sinus rhythm (heart rate = 385 beats per minute).* ***d,*** *Sinus rhythm RR interval (i.e., heart rate) calculated from ECG and gEG.* ***e,*** *Signal-to-noise ratio (SNR) comparison. All the graphene electrodes were in a unipolar window setup but with different window diameters. The intragroup comparison (i.e., ECG vs. gEG) was calculated with a nonparametric Wilcoxon test at a significance level of $p < 0.05$. The intergroup (i.e., 1- vs. 1.5- vs. 2 mm gEG) comparison was calculated with a nonparametric Kruskal-Wallis test in conjunction with Dunn's multiple comparison test at a significance level of $p < 0.05$. $n = 6$ hearts for each group. P-value = 0.0242 (1 mm gEG vs. 2 mm gEG). P-value = 0.0312 (2 mm ECG vs. 2 mm gEG).* ***f,*** *Cardiac pacing (pulse duration = 2 ms, pulse amplitude = 2.5 V, cycle length = 150 ms) was achieved by using the GET-electrode.* ***g,*** *The ex vivo pacing strength-duration curve. $n = 6$ hearts for each group. Data are presented with error bars as mean ± SD. RA, right atrium; LA, left atrium; RV, right ventricle; LV, left ventricle; Pt, platinum; G, graphene.*

Validation of GET-electrodes with optical mapping studies

Graphene is an optically transparent material[28] and has been reported to make transparent electrodes for applications such as photovoltaics[50]. Cardiac optical mapping is a fluorescent imaging technique frequently used in cardiac physiology to study the excitation-contraction coupling between transmembrane potential and calcium handling using optical dyes that emit fluorescence upon excitation illumination[51,52]. Considering the almost complete transparency of graphene and the previous characterization of the sensing and actuating properties of GET-electrodes, it is natural to incorporate GET-electrodes into optical mapping studies where the transmission of light is critically important. It is common to use metal electrodes such as those made of platinum to stimulate the heart during experiments. However, this pacing electrode optically blocks the partial area of the tissue preventing optical recordings. Depending on the size of the electrode, it may be difficult (*e.g.,* low optical signal amplitude, distorted signal morphology) or even impossible to analyze signals from pixels in the region of interest. By using the transparent GET-electrode, those issues are now resolved.

Here we measured and compared the cardiac restitution properties recorded (Fig. 4a) from optical signals (*i.e.,* action potentials and intracellular calcium transients) during pacing by a unipolar GET-electrode (1 mm window size) and a custom bipolar platinum electrode. The GET-electrode, which was placed on the anterior side of the left ventricular surface of the heart, could barely be seen in a bright-field image captured by the camera (Fig. 4b). The activation map showed the expected anisotropic propagation of the transmembrane potential originating from the site of cardiac pacing by GET-electrode throughout the ventricular myocardium (Fig. 4c). Clear representative optical signals from different heart locations, including where the GET-electrode was aligned well with the simultaneously recorded ECG (Fig. 4d). The wide and high-amplitude QRS complex immediately after each pacing artifact indicated successful ventricular capture by the GET-electrode. No statistical difference (see Fig. 4e) was found between the platinum and graphene group of action potential duration 80 (APD80), calcium transient decay constant (Ca Tau), as well as longitudinal and transverse conduction velocity (CVL, CVT). Taken together, these tests indicate that the flexible and transparent GET-electrode is readily applicable to optical mapping studies with high efficacy in cardiac pacing and no harm to the light transmission that allows precise measurement of cardiac restitution properties. Besides, we tested the GET-electrodes for potential cross-connection and insulation performance. As one can see from the

control experiments (see Fig. S4), samples without graphene or passivation opening yield no ECG recording, ensuring that the signal originates specifically from graphene.

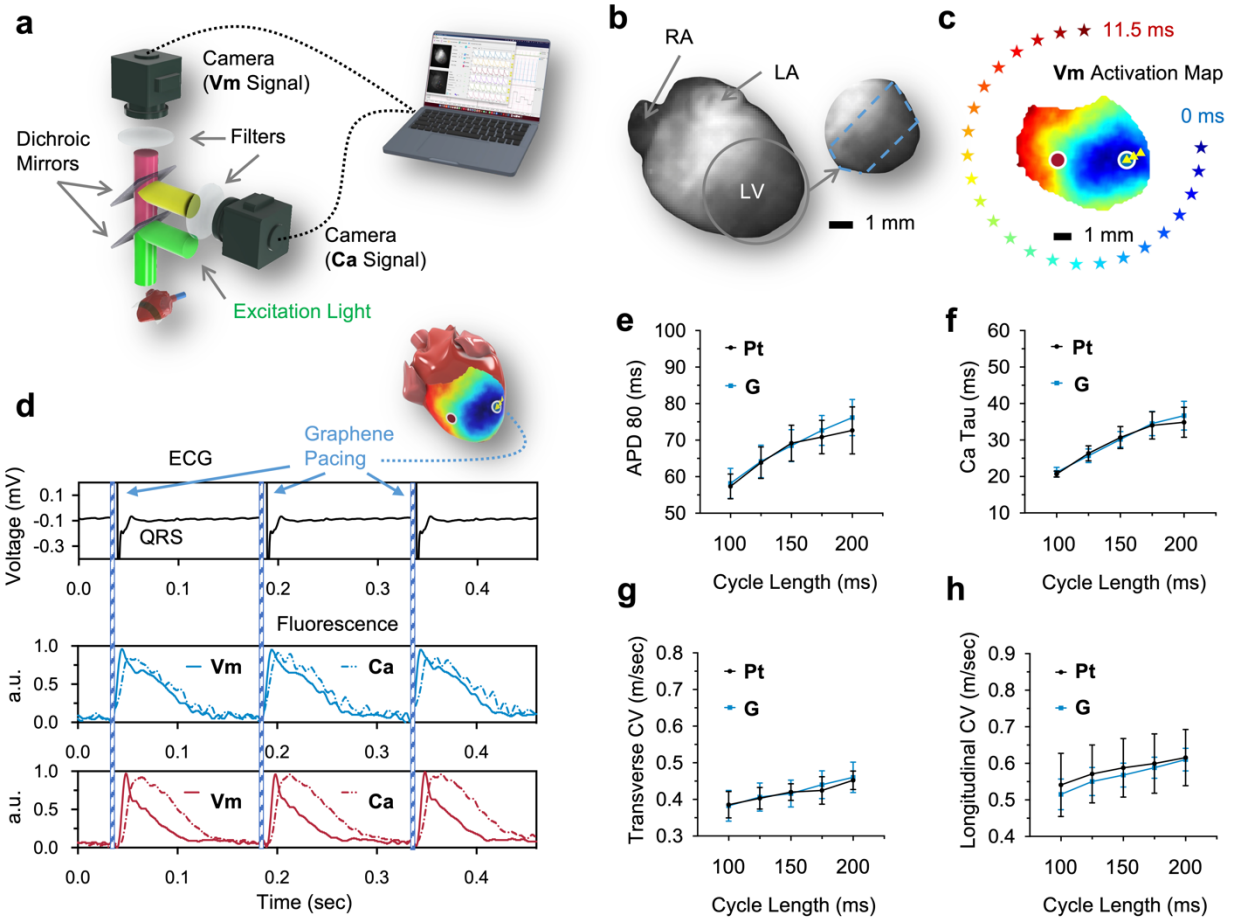

Figure 4 Combination of graphene electrodes with optical mapping studies. a, *Epi-illumination optical mapping system configuration and the light path for Vm and Ca signals. The Langendorff perfused heart was stained with voltage (RH237) and calcium (Rhod-2 AM) sensitive dyes. Emission fluorescence, separated by wavelength using dichroic mirrors and optical filters, was recorded using two CMOS cameras with 100 × 100 pixels resolution (ULTIMA-L, SciMedia) at 2 kHz sampling frequency.* ***b****, Optical mapping camera view of a mouse heart with a magnified view of the heart's left ventricle on which a transparent unipolar (1 mm window size) GET-electrode was placed. The edge of graphene is highlighted with blue dashed lines.* ***c,*** *Activation map of the transmembrane potential during electrical stimulation by the GET-electrode. The yellow triple-triangle symbol marks the location of the electrode window of the GET-electrode. The electrical stimulation is performed right at the spot of the electrode opening (blue circle). The blue and red circles mark the location from which representative traces of Vm and Ca (solid and dashed traces, respectively) were recorded (d).* ***d,*** *Simultaneously recorded ECG and optical signals. The wide QRS complex aligned well with optical signals, which represents successful ventricular activation upon cardiac pacing (pacing pulse duration= 2 ms, pulse amplitude = 4.5 V, cycle length = 150 ms).* ***e-h,*** *Summary restitution properties of the four parameters measured simultaneously by optical mapping. Nonlinear regression analysis was performed on APD80 (**e**), Ca Tau (**f**), CVT (**g**), and CVL (**h**) using the least-squares regression fitting method. An exponential curve* $Y = Y_M - (Y_M - Y_0) * e^{-K*X}$ *was used. Goodness-of-fit was determined by r-squared value > 0.5. The null hypothesis, whether*

one curve adequately fitted all data sets, was tested with the extra sum-of-squares F test at a significance level of $p < 0.05$. $n = 6$ hearts for both platinum and graphene groups. Data were presented with error bars as mean ± SD. RA, right atrium; LA, left atrium; LV, left ventricle; Pt, platinum; G, graphene.

GET-electrode-array for cardiac electrical mapping

Electrical mapping with the high spatial resolution is critical during cardiac EP studies required to guide ablation therapy of arrhythmias. For example, unsatisfactory spatial resolution can result in the incorrect location of drivers of atrial fibrillation (AF), which is the most common type of cardiac arrhythmia affecting millions of patients[53]. To prove the potential high spatial resolution cardiac electrical mapping ability of electrodes based on GETs, we fabricated a novel array of micropatterned GETs (mGETs) and showcased its sensing ability on an *in vivo* beating rat heart (Fig. 5a-c). Unlike earlier version GETs with a whole graphene layer supported by a layer of ultrathin (200 nm) PMMA, the mGETs (Fig. 5a) had two unique features. First, the layer of graphene was patterned into multiple feedlines and individually addressed, all being supported by a single PMMA substrate. Secondly, the mGET-arrays were additionally passivated on top with another layer of PMMA with openings only at the contact and electrode opening sites (like classic microelectrode arrays). However, this PMMA-graphene-PMMA stack resulted in thinnest even microelectrode array, with a thickness below 500 nm.

Moreover, the mm-scale of the devices allowed us to fabricate the devices using off-the-shelf, low-cost additive fabrication components (see Methods). The 2 × 2 mGET-arrays were placed on a rat heart to record electrical signals from both right and left ventricles (Fig. 5a-c). *In vivo* ECG was recorded throughout the period of the experiments from sensing electrodes positioned in the lead II configuration. One can see prominent PQRST phases of a healthy cardiac wave. Because one graphene electrode (Fig. 5c, gEG-4) was placed close to the atrium, a clear P wave was observed. The simultaneously recorded ECG and gEG showed a good temporal correlation of R waves. Figure S5 shows the four gEGs individually.

Treating atrioventricular block (AV block) in an *in vivo* rat model

Fig. 5d shows the *in vivo* pacing strength-duration curve of bipolar GET-electrodes. Stimulus pulse duration covered the clinically used values such as from 0.2 to 0.5 ms[47–49]. Fig. 5e-g shows the application of the bipolar GET-electrode to the treatment of AV block. AV block was induced by fast pacing (cycle length 100ms) at the left ventricle after intraperitoneal injection of 120 mg/kg caffeine and 60 mg/kg dobutamine. When no pacing treatment was applied, the rat heart exhibited

continuous 4:1 AV block (Fig. 5e-f). Upon ventricular pacing using mGET-arrays (pacing heart rate at 300 BPM), successful capture with clear pacing spikes and widen morphologies of the QRS complex was observed (Fig. 5g). The ventricular beating was also apparent during pacing compared with almost silent contraction during AV block (photographs not shown here). When pacing was stopped, the heart rhythm returned to AV block (Fig .5e, brown box). Overall, these *in vivo* tests demonstrate that the flexible mGET-arrays can effectively sense and capture a beating heart that has the potential to be applied to clinically relevant scenarios like ventricular rhythm normalization during common arrhythmias such as AV block. This is the first time graphene electrodes have been used to successfully treat a life-threatening heart rhythm disorder.

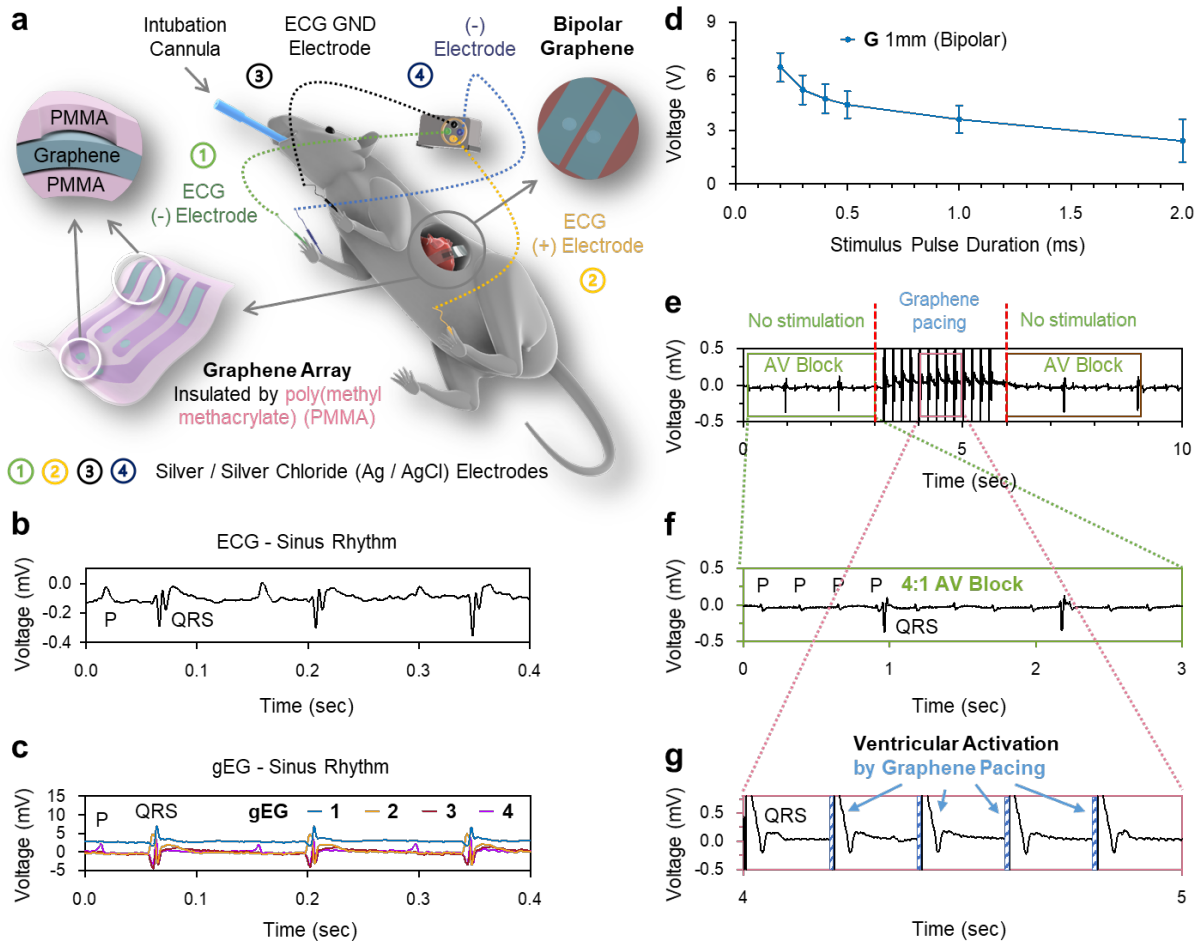

Figure 5 Cardiac electrical mapping and treatment of AV block in an in vivo rat model. a, *Schematic of the in vivo study setup. ECG was recorded through subdermal needle electrodes positioned in the Lead II configuration. Electrogram was recorded using the 2-by-2 mGET-array-electrode (the magnified view shows an electrode array of two PMMA layers highlighted with purple color and graphene in light blue). Electrode window size of each graphene feedline = 1 mm. The window pitch distance = 6 mm. For the bipolar GET-electrode, 1 mm window size and 2 mm window pitch distance was used. The GET-array-*

electrode could simultaneously record gEG from both the right and left ventricles of the heart. ***b-c,*** *Simultaneously recorded ECG (**b**) and four gEGs from four electrodes within one array (**c**) at natural sinus rhythm (heart rate = 425 beats per minute). gEG-4 showcases the ability to record atrial electrical signals (i.e., P wave) when the graphene electrode is placed near the atrium.* ***d,*** *In vivo pacing strength-duration curve using bipolar GET-electrodes. In bipolar pacing mode, one and the other graphene electrodes were used as (+) and (-) electrodes, respectively, on n = 6 hearts.* ***e-g,*** *In vivo ECG monitoring of a rat heart with 4:1 AV block before cardiac pacing (green box), regular ventricular activity during pacing (cycle length = 200 ms, pacing pulse duration = 2 ms, pulse amplitude = 2.5 V) (pink box), and AV block when pacing was stopped (brown box). Ventricular capture via electrical stimulation was observed as the wide QRS complex after each pacing artifact. G, graphene.*

Conclusions

Bioelectronics has revolutionized cardiology and cardiac physiology by enabling electrocardiography, arrhythmia diagnostics, anti-arrhythmia ablation, and implantable device therapies. The diagnosis and treatment of cardiac diseases (*i.e.,* arrhythmias, myocardial infarction, and heart failure) have also been facilitated since the arrival and evolution of essential tools such as cardiac pacemakers and defibrillators[48,54]. In recent years, the conventional bulky and rigid cardiac devices and catheters show a clear trend of becoming smaller, softer, portable, and multifunctional by engineering better materials or designing more sophisticated fabrication methods. Yet, there is still no technology capable of seamless integration with the perpetually undulating cardiac tissue that would robustly enable electrical sensing and actuation of the tissue properties.

In this study, we report on a distinct class of soft and transparent bioelectronics fabricated using graphene electronic tattoos. The sub-micrometer thickness and softness of graphene tattoos make them superior for seamless coupling with the cardiac tissue, yielding unique elements of soft bioelectronics that conform well to the heart without constraining or altering its natural motions. Electrochemical properties, including interface impedance, charge storage capacity, and charge injection capacity of the reported 500 nm thick PMMA-supported and passivated graphene biointerfaces are superior to most emerging technologies (see Table S1). While sensing and actuating cardiac tissue, leveraging transparency of graphene biointerfaces, we can simultaneously perform optocardiography, *i.e.,* using light to sense and stimulate electrical or metabolic dynamics of the heart, as demonstrated here *via* a set of systematic *ex vivo* and *in vivo* animal studies. Most importantly, we show that the graphene biointerfaces can effectively diagnose and treat a common clinical arrhythmia**,** AV block, in a rat model, signifying their superiority for high-density electrical pace-mapping, and leading to advanced diagnosis and treatment of cardiac arrhythmias.

Methods

Preparation of three-layer graphene tattoo. Graphene requires adequate protection and support, provided using the ultrathin layer of PMMA. High-quality monolayer graphene is grown *via* the CVD method on a copper foil (Grolltex), fixed on a Si wafer, and then a layer of PMMA (950 A4) is spin-coated at 2500rpm for 60 seconds, followed by 200℃ bake on the hotplate for 20 min. Copper was removed by placing the PMMA/graphene/copper in 0.1 M $(NH_4)_2S_2O_8$ solution for 8-12h. The floating PMMA-graphene was then picked up by a Si wafer (must be larger than the piece of PMMA/graphene flake) and transferred into DI water in three stages (5min, 5min, and 30min) to remove any residual copper etchant solution. The PMMA/graphene piece was then picked up by a new piece of clean 1L graphene/copper, and the process was repeated. PMMA-graphene-graphene-copper was air-dried overnight at room temperature in a hood. Two-layer graphene was produced by annealing the PMMA-graphene-graphene-copper on a 200℃ hot plate. The copper foil of the 2-layer graphene was also removed by putting it in 0.1 M $(NH_4)_2S_2O_8$ solution for 8-12h. 3-layer graphene on copper foil was fabricated by repeating the preceding steps. Using two sheets of tattoo paper (Silhouette Cameo), transfer PMMA/graphene and flip to have an arrangement with graphene facing up[40].

Cut the graphene tattoo into 15mm*3mm strips. The graphene tattoo was attached to Silhouette Cameo cutting mat using Kapton tape. A Cameo plotter was used to cut the graphene tattoo into 15mm*3mm strips (Cut Through: Depth 2, Pressure 25; Scoring Surface: Depth 1, Pressure 15). To get a clean designed shape, immerse the graphene tattoo in water for about 30 seconds, use tweezers to remove unwanted parts, and separate each graphene strip.

Preparation of graphene electrode. 10% (g/ml) poly(vinyl alcohol) (PVA) (Millipore Sigma, catalog number 341584) was spin-coated (100 rpm, 500 acceleration) for 40 sec onto a glass substrate and cured at room temperature (20~22 °C) for 48 hours. The water-soluble PVA layer served as a temporary supporting layer to ease the delamination of the encapsulation layer (made from Ecoflex silicones) from the glass substrate. Ecoflex™ 00-30 (Smooth-On) silicones were prepared by mixing Ecoflex monomer and curing agent (volume-to-volume, v/v = 1:1). Vacuum degassing was applied for 5~10 minutes until bubbles were cleared. The liquid silicones were spin-coated (100 rpm, 500 acceleration) for 60 sec on top of the PVA layer and cured at room temperature for 48 hours. The electrode window with a desired diameter and pattern was created by cutting through the silicone encapsulation layer with biopsy punches. The unipolar pattern had an electrode window size of 1-, 1.5-, and 2 mm. The bipolar pattern had two 1 mm electrode windows with a pitch distance of 2 mm. The 2 × 2 array pattern had four 1 mm electrode windows with a pitch distance of 6 mm. A gold tape worked as the interconnect and was gently placed on top of the silicone encapsulation layer. And the graphene tattoo was gently placed in such a way that one of its ends covered the electrode window, and the other end contacted the gold tape. Another layer of silicone encapsulation was prepared as aforementioned. Just before use, the graphene electrode was gently peeled off from the glass substrate, and the PVA layer was washed off by 1X PBS solution.

Electrical Impedance Characterization.

The EIS, CV, CSC, and CIC characterization was performed on CEC Autolab TGSTAT 128N in a three-electrode system. Graphene was connected as the working electrode (WE), the platinum wire as the counter electrode (CE), and a 2.0mm diameter Ag/AgCl pellet as the reference electrode (RE), all immersed in PBS×1 solution. The graphene electrode was connected by gold tape and conductive silver epoxy. *For EIS measurements*, 10 mV sine waves at frequencies from 1 Hz to 100 kHz were applied. *For CV measurements,*

the potential sweep from −0.9 to 1.2 V was applied, which is a water window, and the cycle curve was plotted to show the stabilized signal, with scan rates ranging from 5 to 1000 mV/s.

To estimate charge storage capacity (CSC), the CV curve which at water window with a scan rate of 5 mV/s was used. The cathodic and anodic areas were integrated, and the area difference was calculated. The area-normalized CSC was obtained by dividing the calculated area difference by the exposed geometric area of the devices. *For charge injection capacity (CIC) measurements,* charge-balanced, constant-current pulses with a current range from 0.1μA to 5μA, cathode leading, 0.5s long phases, and 5s gap between phases were applied to the WE (return path through the CE). The resulting voltage transient was measured between the WE and RE. The maximum negative polarization potential (Emc) was assumed to be the WE voltage at the end of the cathodic/anodic phase.

Animals. The George Washington University Institutional Animal Care and Use Committee approved all experimental animal protocols. The procedures were by suggestions from the panel of Euthanasia of the American Veterinary Medical Association and the National Institutes of Health Guide for the Care and Use of Laboratory Animals. *Ex vivo* studies were performed on mouse (15~25 weeks old; C57BL/6J; Jackson Labs stock # 000664; male and female) hearts. *In vivo* studies were performed on Sprague-Dawley rats (15~20 weeks old; Hilltop Lab Animals; female)

Langendorff perfusion of the heart. Mice were anesthetized by 3% (volume-to-volume, v/v) isoflurane inhalation until the animal no longer responded to a toe pinch. The cervical dislocation was quickly performed before thoracotomy. The heart was excised and retrogradely perfused *via* aortic cannulation inside a temperature-controlled (37 °C) Langendorff perfusion system. A modified Tyrode's solution (in mM, NaCl 140, KCl 4.7, $MgCl_2$ 1.05, $CaCl_2$ 1.3, Glucose 11.1, HEPES 10, pH 7.4 at 37 °C) bubbled with 100% O_2 was used, and the perfusion pressure was maintained at 70~90 mmHg by adjusting the flow rate between 1 and 2.5 ml/min.

Pacing strength-duration curve characterization. A platinum bipolar electrode (A-M Systems, catalog number 778000) was used for *ex vivo* studies; and various (1 mm bipolar; 1-, 1.5- 2 mm unipolar) graphene electrodes were used for ex- and *in vivo* studies. Electrodes were placed at the anterior center of the left ventricular surface. Stimulating monophasic square pulses with different pulse duration (ms) and pulse amplitude (volt) were generated by a pulse generator (ADInstruments, PowerLab 26T). For mouse (*ex vivo*) and rat (*in vivo*) hearts, the stimulating pacing cycle length of 150 ms (*i.e.,* 400 beats per minute heart rate) and 125 ms (*i.e.,* 480 beats per minute heart rate) were used, respectively. The stimulating pulse amplitude ranged from 0 to 20 V as the pulse generator could afford and was increased in a 0.1 V step. The pacing threshold was defined as the minimal voltage that could pace the heart for at least 10 consecutive beats.

***Ex vivo* far-field pseudo-electrocardiogram (ECG) and graphene-electrogram (gEG) recording.** Both *ex vivo* ECG and gEG signals were acquired using PowerLab 26T and LabChart software (ADInstruments) when the heart was perfused inside the Langendorff chamber. ECG was recorded using a 3-sensing electrodes setup: a positive electrode was placed near the right atrium, a ground electrode was placed near the left atrium, and a negative electrode was placed near the apex of the heart. gEG was recorded using a 2-sensing electrodes setup: a positive electrode (*i.e.,* GET-electrode) was placed on the anterior surface of the heart, and a negative electrode was placed near the left atrium.

***In vivo* ECG and gEG recording.** In vivo ECG and gEG signals were acquired using PowerLab 26T and LabChart software (ADInstruments). ECG was recorded using a 3-sensing electrodes setup in the Lead II

configuration: a subdermal positive electrode was placed in the left leg, a subdermal ground electrode was placed in the left arm, and a subdermal negative electrode was placed in the right arm. gEG was recorded using a 2-sensing electrodes setup: a positive electrode (*i.e.,* GET-electrode) was placed on the anterior-lateral surface of the heart, and a subdermal negative electrode was placed on the right arm.

Optical mapping. Optical mapping was performed as previously described[55]. The cardiac contraction was arrested with 10~13 μM blebbistatin (Cayman Chemicals, catalog number 13186), an electromechanical uncoupler, for 15~20 min before loading the voltage-sensitive dye RH237 (1.25 mg/ml dye stock solution in DMSO, Biotium, catalog number 61018) and calcium-sensitive dye Rhod-2 AM (1 mg/ml dye stock solution in DMSO, Thermo Fisher Scientific, catalog number R1244). The heart was subjected to a 15 min equilibration period followed by dye staining to allow the washout of extra dye. The heart was illuminated by an LED at 520 +/- 17 nm wavelength. Voltage fluorescence signals (filtered by a 695 nm long-pass filter) and calcium fluorescence signals (filtered by a 572 +/- 14 nm band-pass filter) were simultaneously acquired by two CMOS cameras with 100 × 100 pixels resolution (ULTIMA-L, SciMedia) at 2 kHz sampling frequency. The field of view of the camera was 15 × 15 mm. The platinum bipolar electrode or the 1 mm unipolar graphene electrode was placed at the center of the anterior surface of the mouse heart. Electrical stimuli (with 2 ms pulse duration) were applied to determine the pacing voltage threshold. And the heart was paced at 1.5X pacing voltage threshold and 2 ms pulse duration. The pacing cycle length (in ms, 200, 175, 150, 125, 100) was varied to determine the cardiac restitution properties.

Optical data analysis. Optical data of transmembrane potential and calcium were analyzed using a custom MATLAB (R2021a) software. Four different parameters were measured. These include (1) action potential duration 80 (APD80) - the time interval from the activation time (*i.e.,* time of maximum 1st derivative of the upstroke) to 80% repolarization, (2) calcium decay time constant (Ca Tau, τ) - a value calculated by fitting an exponential curve ($F(t) = e^{\frac{-1}{\tau}*t} + A$) to the calcium transient decay phase (from 30% to 90% decay), (3) transverse and (4) longitudinal conduction velocity (CVT and CVL) were in parallel and perpendicular to the cardiac fiber direction. These two parameters were calculated using differences in activation times and the known interpixel distances.

***In vivo* rat study.** Surgery procedures were performed as previously described[56]. All the surgical procedures were performed under general anesthesia with 3% (v/v) isoflurane inhalation until the animal no longer responded to a toe pinch. The rat was intubated by a 16-gauge cannula and was ventilated using a VentElite small-animal ventilator (Harvard Apparatus, catalog number 55-7040) at a ventilation rate of 80 breaths per minute under pressure control mode with the peak inspiratory pressure limit of 14 cmH_2O. After the left thoracotomy, the lung was gently retracted by a cotton swab to expose the heart. The pericardium was gently removed using another cotton swab.

In vivo ECG monitoring was performed as aforementioned. For the pacing purpose, a 1 mm bipolar graphene electrode was placed at the anterior-lateral side of the left ventricular surface. Atrioventricular node block (AV block), one kind of cardiac arrhythmia, was induced using a previously described method[55]. Briefly, the rat received (intraperitoneally, IP) 120 mg/kg caffeine (Millipore Sigma, catalog number C0750) and 60 mg/kg dobutamine (Cayman, catalog number 15582) sequentially. Fast pacing (cycle length 100 ms) at the left ventricle was applied for about 15 minutes after drug treatment until AV block was seen. Baseline sinus rhythm was recorded before drug treatment. AV block recording and cardiac rhythm conversion *via* graphene electrode pacing were performed. The PowerLab 26T was used as the energy

source to stimulate the heart. After finishing the study, a very deep level of anesthesia was confirmed, the heart was excised, and euthanasia was achieved by exsanguination.

Statistical analysis. Results are reported as mean +/- standard deviation (SD) unless otherwise noted. Statistical analyses were performed using statistical software (Graphpad Prism, ver 8.4.3). For signal-to-noise ratio analysis, intragroup (*i.e.,* ECG vs. gEG) significance was calculated with a nonparametric Wilcoxon test at a significance level of $p < 0.05$; and intergroup (*i.e.,* 1- vs. 1.5- vs. 2 mm gEG) significance was calculated with a nonparametric Kruskal-Wallis test in conjunction with Dunn's multiple comparison test at a significance level of $p < 0.05$. Nonlinear regression analysis was performed on APD80, Ca Tau, CVT, and CVL using the least-squares regression fitting method. An exponential curve $Y = Y_M - (Y_M - Y_0) * e^{-K*X}$ was used. Goodness-of-fit was determined by r-squared value > 0.5. The null hypothesis, whether one curve adequately fitted all data sets, was tested with the extra sum-of-squares F test at a significance level of $p < 0.05$.

Acknowledgments

This research was supported by NIH grants R21-HL152324, 3OT2OD023848, and R01 HL141470; and Leducq Foundation grant RHYTHM. D.A acknowledges the support of the Office of Naval Research (ONR) under grant number N00014-18-1-2706, and the Temple Foundation Endowed Professorship.

Author contributions

Z.L., D.K., and I.E. conceived the overall research goals and objectives. Z.L. and D.K. performed proof-of-concept experiments. D.K. and N.L. designed and fabricated GETs and GET arrays. Z.L., S.N.O., and Z.C. conceived and executed the prototyping of the device design. Z.L. performed soft GET-electrodes fabrication. Z.L. performed *ex vivo* experiments. Z.L. and J.L. performed *in vivo* experiments. N.L. and D.K. performed electrochemical impedance measurements. Z.L. and S.G. performed data analysis. D.K. and N.L. performed electrochemical data analysis. Z.L., D.K., N.L., D.A., and I.E. wrote the manuscript. I.E. and D.A. provided funding. All authors reviewed the manuscript before submission.

Competing interests

The authors declare no competing financial interest.

References

1. SMITH, H. J. *et al.* Five-Years Experience with Intravascular Lead Extraction. *Pacing Clin. Electrophysiol.* **17**, (1994).
2. Türkan, U., Öztürk, O. & Eroğlu, A. E. Metal ion release from TiN coated CoCrMo orthopedic implant material. *Surf. Coatings Technol.* **200**, (2006).
3. Feiner, R. & Dvir, T. Tissue-electronics interfaces: From implantable devices to engineered tissues. *Nature Reviews Materials* **3**, (2017).
4. Cho, K. W. *et al.* Soft Bioelectronics Based on Nanomaterials. *Chemical Reviews* **122**, (2022).
5. Cox-Pridmore, D. M., Castro, F. A., Silva, S. R. P., Camelliti, P. & Zhao, Y. Emerging Bioelectronic Strategies for Cardiovascular Tissue Engineering and Implantation. *Small* (2022). doi:10.1002/smll.202105281
6. Feron, K. *et al.* Organic bioelectronics: Materials and biocompatibility. *International Journal of Molecular Sciences* **19**, (2018).
7. Inal, S., Rivnay, J., Suiu, A. O., Malliaras, G. G. & McCulloch, I. Conjugated Polymers in Bioelectronics. *Acc. Chem. Res.* **51**, (2018).
8. Lacour, S. P., Courtine, G. & Guck, J. Materials and technologies for soft implantable neuroprostheses. *Nat. Rev. Mater.* **1**, 16063 (2016).
9. Sunwoo, S. H., Ha, K. H., Lee, S., Lu, N. & Kim, D. H. Wearable and Implantable Soft Bioelectronics: Device Designs and Material Strategies. *Annu. Rev. Chem. Biomol. Eng.* **12**, 359–391 (2021).
10. Sunwoo, S. H. *et al.* Advances in Soft Bioelectronics for Brain Research and Clinical Neuroengineering. *Matter* **3**, (2020).
11. Tang, X., He, Y. & Liu, J. Soft bioelectronics for cardiac interfaces. *Biophys. Rev.* **3**, (2022).
12. Bettinger, C. J. & Bao, Z. Biomaterials-based organic electronic devices. *Polymer International* **59**, (2010).
13. Someya, T., Bao, Z. & Malliaras, G. G. The rise of plastic bioelectronics. *Nature* **540**, (2016).
14. Liu, Y., Pharr, M. & Salvatore, G. A. Lab-on-Skin: A Review of Flexible and Stretchable Electronics for Wearable Health Monitoring. *ACS Nano* **11**, (2017).
15. Ray, T. R. *et al.* Bio-Integrated Wearable Systems: A Comprehensive Review. *Chem. Rev.* **119**, 5461–5533 (2019).
16. Gutruf, P. *et al.* Wireless, battery-free, fully implantable multimodal and multisite pacemakers for applications in small animal models. *Nat. Commun.* **10**, (2019).
17. Han, M. *et al.* Catheter-integrated soft multilayer electronic arrays for multiplexed sensing and actuation during cardiac surgery. *Nat. Biomed. Eng.* **4**, 997–1009 (2020).
18. Choi, Y. S. *et al.* Fully implantable and bioresorbable cardiac pacemakers without leads or batteries. *Nat. Biotechnol.* **39**, 1228–1238 (2021).
19. Chen, Z. *et al.* Flexible and Transparent Metal Nanowire Microelectrode Arrays and Interconnects for Electrophysiology, Optogenetics, and Optical Mapping. *Adv. Mater. Technol.* **6**, (2021).
20. Choi, Y. S. *et al.* A transient, closed-loop network of wireless, body-integrated devices for autonomous electrotherapy. *Science (80-.).* **376**, 1006–1012 (2022).
21. Yang, Q. *et al.* Photocurable bioresorbable adhesives as functional interfaces between flexible bioelectronic devices and soft biological tissues. *Nat. Mater.* (2021).

doi:10.1038/s41563-021-01051-x
22. Park, J. *et al.* Electromechanical cardioplasty using a wrapped elasto-conductive epicardial mesh. *Sci. Transl. Med.* **8**, (2016).
23. Rastogi, S. K. *et al.* Three-dimensional fuzzy graphene ultra-microelectrodes for subcellular electrical recordings. *Nano Res.* **13**, (2020).
24. Lin, Z. C., Xie, C., Osakada, Y., Cui, Y. & Cui, B. Iridium oxide nanotube electrodes for sensitive and prolonged intracellular measurement of action potentials. *Nat. Commun.* **5**, 3206 (2014).
25. Liu, H. *et al.* Heart-on-a-Chip Model with Integrated Extra- And Intracellular Bioelectronics for Monitoring Cardiac Electrophysiology under Acute Hypoxia. *Nano Lett.* **20**, (2020).
26. Liu, Y. *et al.* Soft conductive micropillar electrode arrays for biologically relevant electrophysiological recording. *Proc. Natl. Acad. Sci. U. S. A.* **115**, (2018).
27. Novoselov, K. S. S. *et al.* Electric field effect in atomically thin carbon films. *Science* **306**, 666–9 (2004).
28. Nair, R. R. *et al.* Fine Structure Constant Defines Visual Transparency of Graphene. *Science (80-.).* **320**, 1308–1308 (2008).
29. Lee, C., Wei, X., Kysar, J. W. & Hone, J. Measurement of the elastic properties and intrinsic strength of monolayer graphene. *Science (80-.).* **321**, (2008).
30. Jang, H., Dai, Z., Ha, K.-H., Ameri, S. K. & Lu, N. Stretchability of PMMA-supported CVD graphene and of its electrical contacts. *2D Mater.* **7**, 014003 (2019).
31. Pampaloni, N. P. *et al.* Single-layer graphene modulates neuronal communication and augments membrane ion currents. *Nat. Nanotechnol.* **13**, 755–764 (2018).
32. Fabbro, A. *et al.* Graphene-Based Interfaces Do Not Alter Target Nerve Cells. *ACS Nano* **10**, 615–623 (2016).
33. Kireev, D. & Offenhaeusser, A. Graphene & two-dimensional devices for bioelectronics and neuroprosthetics. *2D Mater.* **5**, 042004 (2018).
34. Talebi, A., Labbaf, S., Karimzadeh, F., Masaeli, E. & Nasr Esfahani, M. H. Electroconductive Graphene-Containing Polymeric Patch: A Promising Platform for Future Cardiac Repair. *ACS Biomater. Sci. Eng.* **6**, (2020).
35. Dipalo, M. *et al.* Intracellular action potential recordings from cardiomyocytes by ultrafast pulsed laser irradiation of fuzzy graphene microelectrodes. *Sci. Adv.* **7**, (2021).
36. Kireev, D. *et al.* Versatile Flexible Graphene Multielectrode Arrays. *Biosensors* **7**, 1 (2016).
37. Kuzum, D. *et al.* Transparent and flexible low noise graphene electrodes for simultaneous electrophysiology and neuroimaging. *Nat. Commun.* **5**, 5259 (2014).
38. Masvidal-Codina, E. *et al.* High-resolution mapping of infraslow cortical brain activity enabled by graphene microtransistors. *Nat. Mater.* **18**, 280–288 (2019).
39. Bonaccini Calia, A. *et al.* Full-bandwidth electrophysiology of seizures and epileptiform activity enabled by flexible graphene microtransistor depth neural probes. *Nat. Nanotechnol.* **17**, (2022).
40. Kireev, D. *et al.* Fabrication, characterization and applications of graphene electronic tattoos. *Nat. Protoc.* **16**, 2395–2417 (2021).
41. Kabiri Ameri, S. *et al.* Graphene Electronic Tattoo Sensors. *ACS Nano* **11**, 7634–7641 (2017).
42. Kireev, D. *et al.* Continuous Cuffless Monitoring of Arterial Blood Pressure via Graphene

Bioimpedance Tattoos. *Nat. Nanotechnol.* (2022). doi:10.1038/s41565-022-01145-w

43. Kireev, D., Kampfe, J., Hall, A. & Akinwande, D. Graphene Electronic Tattoos 2.0 with Enhanced Performance, Breathability and Robustness. *npj 2D Mater. Appl.* (2022).
44. Kireev, D. *et al.* Multipurpose and Reusable Ultrathin Electronic Tattoos Based on PtSe 2 and PtTe 2. *ACS Nano* **15**, 2800–2811 (2021).
45. Park, D.-W. W. *et al.* Graphene-based carbon-layered electrode array technology for neural imaging and optogenetic applications. *Nat. Commun.* **5**, 5258 (2014).
46. Park, D.-W. *et al.* Electrical Neural Stimulation and Simultaneous in Vivo Monitoring with Transparent Graphene Electrode Arrays Implanted in GCaMP6f Mice. *ACS Nano* **12**, 148–157 (2018).
47. Boriani, G. *et al.* Role of ventricular autocapture function in increasing longevity of DDDR pacemakers: A prospective study. *Europace* **8**, (2006).
48. Mulpuru, S. K., Madhavan, M., McLeod, C. J., Cha, Y.-M. & Friedman, P. A. Cardiac Pacemakers: Function, Troubleshooting, and Management. *J. Am. Coll. Cardiol.* **69**, (2017).
49. Doukky, R., Bargout, R., Kelly, R. F. & Calvin, J. E. Using transcutaneous cardiac pacing to best advantage: How to ensure successful capture and avoid complications. *J. Crit. Illn.* **18**, (2003).
50. Fernández, S. *et al.* Advanced graphene-based transparent conductive electrodes for photovoltaic applications. *Micromachines* **10**, (2019).
51. Efimov, I. R., Nikolski, V. P. & Salama, G. Optical imaging of the heart. *Circulation Research* **95**, (2004).
52. O'Shea, C. *et al.* Cardiac optical mapping – State-of-the-art and future challenges. *International Journal of Biochemistry and Cell Biology* **126**, (2020).
53. Roney, C. H. *et al.* Spatial Resolution Requirements for Accurate Identification of Drivers of Atrial Fibrillation. *Circ. Arrhythmia Electrophysiol.* **10**, (2017).
54. DeForge, W. F. Cardiac pacemakers: a basic review of the history and current technology. *J. Vet. Cardiol.* **22**, (2019).
55. George, S. A., Lin, Z. & Efimov, I. R. Simultaneous triple-parametric optical mapping of transmembrane potential, intracellular calcium and NADH for cardiac physiology assessment. *Commun. Biol.* **5**, 1–10 (2022).
56. Yin, R. T., Chen, S. W., George, T., Lee, K. B. & Murillo-berlioz, A. *Open thoracic surgical implantation of cardiac pacemakers in rodents*. doi:10.21203/rs.3.pex-1684/v1